Available online at www.sciencedirect.com
ScienceDirect
Lithos 94 (2007) 46–65
LITHOS
www.elsevier.com/locate/lithos

Depleted lithosphere from the mantle wedge beneath Tres Lagos, southern Patagonia, Argentina

Th. Ntaflos [a,*], E.A. Bjerg [b], C.H. Labudia [b], G. Kurat [a]

[a] Department of Lithospheric Sciences, University of Vienna, Althanstrasse 14, A-1090 Vienna, Austria
[b] CONICET-Universidad Nacional del Sur, Departamento de Geología, San Juan 670, B8000ICN Bahía Blanca, Argentina

Received 18 April 2005; accepted 2 June 2006
Available online 22 August 2006

Abstract

Anhydrous spinel lherzolite and harzburgite xenoliths from Tres Lagos, situated inboard of the Volcanic Arc Gap (VAG) in southernmost Patagonia, are samples of a depleted lithospheric mantle and can be divided into two major groups: metasomatized and non-metasomatized. Metasomatized samples, which are the minority, are partly mylonitized and their metasomatism is related to this tectonic process. A group of non-metasomatized samples have enriched whole rock LREE-abundances that are not consistent with the depleted LREE-abundances in their clinopyroxenes. Intergranular host basalt infiltration could be responsible for the whole rock LREE enrichments. Their Sr- and Nd-isotopic ratios have also been affected by host basalt infiltration, whereas their high Sr-isotopic ratios point to subsequent contamination by ground-water and/or Ca-rich surface solutions. Similar contamination is thought to cause the decoupling of Sr- and Nd-isotopes (high Sr- and Nd-isotopic ratios) observed in the non-metasomatized samples with depleted whole rock LREE. A two-stage partial melting process could be responsible for the origin of the Tres Lagos xenoliths. Model calculations have shown that in the first stage, 2% of batch melting took place in the garnet peridotite field and subsequently the residue experienced 2–8% batch melting in the spinel peridotite field. The Tres Lagos peridotites have not been affected by subduction-related metasomatic processes and they could represent an old lithospheric mantle.

Keywords: Alkali basalts; Xenoliths; Upper mantle; Metasomatism; Patagonia

1. Introduction

The lithospheric mantle has undergone a complex history of depletion and enrichment in various elements in response to partial melting and metasomatism, as has been revealed by studies of mantle-derived xenoliths from around the world. Patagonia, the southernmost portion of South America, offers an opportunity to study the present situation in the upper mantle at this latitude as it is covered by geologically young basaltic volcanism, with part of it providing ultramafic xenoliths, direct samples from the upper mantle. In the few past years, new data from Stern et al. (1990, 1999), Kilian et al. (1998), Ntaflos et al. (2002), Gorring and Kay (2000), Kilian and Stern (2002), Rivalenti et al. (2004), Bjerg et al. (2005) and references therein, have contributed to a better understanding of the petrology and geochemistry of the upper mantle in this region, especially about the metasomatic processes that took place (and still take place) in the upper mantle, and about the origin of the fluids responsible for metasomatism.

Tres Lagos is located at the latitude of the Volcanic Arc Gap, east of the subduction zone and the basalts from this locality were reported by Stern et al. (1990) and classified

* Corresponding author. Fax: +43 1 4277 9534.
E-mail address: theodoros.ntaflos@univie.ac.at (T. Ntaflos).

0024-4937/$ - see front matter © 2006 Elsevier B.V. All rights reserved.
doi:10.1016/j.lithos.2006.06.011

in the group of "cratonic" basalts. The xenoliths which occur in these basalts are of particular interest since both metasomatized and non-metasomatized xenoliths occur at volcanic centers that are located close to each other (Ramos, 1999; Gorring and Kay, 2000; Schilling et al., 2005). Here we report new data on a large collection of upper mantle xenoliths from the Tres Lagos volcanic area, which offer a detailed view into the sub-continental upper mantle in this controversial part of Patagonia.

2. Geological setting and sampling locality

The Andean Cordillera represents the western continental margin of the South American Plate, whose geologic evolution is related to subduction of the Nazca and Antarctic plates below South America. South of 39° S, the Andean Cordillera can be divided into two major regions (Fig. 1). The Southern Volcanic Zone (SVZ) extending to 46° S, is followed by a gap in volcanic activity (VAG) due to the Chile Rise–Trench triple junction (Ramos, 1999; Stern, 2004). The latter separates the SVZ from the Austral Volcanic Zone (AVZ), which extends from 49° S to 54° S (Stern and Kilian, 1996). A representative suite of mantle xenoliths from the VAG region was collected in the Santa Cruz province (Fig. 1), at a road cut north of the Tres Lagos locality, along highway Nr. 40 (49°37′ S, 71°30′ W). The xenoliths range in size between 4 and 20 cm, and they occur in lava flows, a cinder cone and basalt "dikes" (40–50 cm wide) cutting the cinder cone. Samples from the cinder cone are colored deep red due to oxidation. Unaltered xenoliths are dominant in basalt flows and dikes. Stern et al. (1990) presented a comprehensive study of the Patagonia basalts, which included geochemistry and isotopic data of Tres Lagos locality.

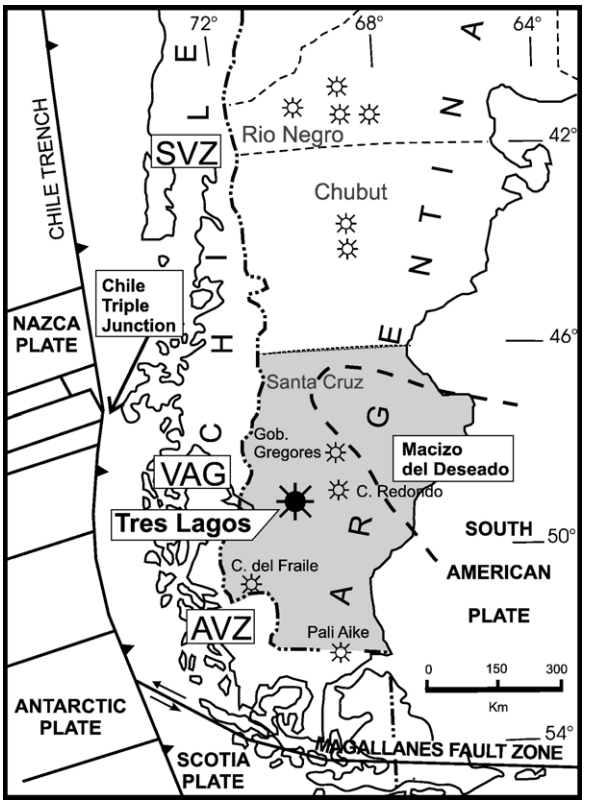

Fig. 1. Location map showing the tectonic setting and occurrences of mantle xenoliths in Río Negro, Chubut and Santa Cruz provinces (modified from Gorring and Kay, 2000; Bjerg et al., 2005). SVZ: Southern Volcanic Zone, VGZ: Volcanic Gap Zone, AVZ: Austral Volcanic Zone.

3. Analytical methods

Electron microprobe analyses of major minerals were carried out with a Cameca SX 100 electron microprobe (University of Vienna, Department of Geological Sciences). All analyses were made against mineral standards by utilizing wavelength-dispersive spectrometers; acceleration voltage and beam current were 15 kV and 15 nA, respectively, and standard correction procedures were applied.

Major and trace element analyses were carried out with XRF techniques (Philips 2400). Th, U and REE were analyzed by ICP-MS techniques (ELAN 6100) at the University of Vienna, Department of Geological Sciences. Sample preparation and Sr and Nd isotopic analytical work was performed at the Laboratory of Geochronology, Department of Lithospheric Sciences, University of Vienna, using the analytical procedure described by Thöni and Miller (2004) and determination of Sr and Nd isotopes was carried out on a Thermo-Finnigan Triton TI TIMS. Xenolith modal proportions were calculated using bulk rock (XRF) and mineral analyses (EMPA).

Trace element contents of minerals were analyzed by laser ablation inductively coupled plasma mass spectrometry at the University of Bristol (LA-ICP-MS, VG Elemental Plasma Quad 3). The laser system was used in pulse mode with a frequency of 10 Hz and energy of about 0.1–0.15 mJ/pulse. The laser beam was 20° μm wide. The spots for analysis were selected under an optical microscope. The NIST 610 and 612 glasses were used as external standard and the CaO content in minerals as the internal standard for yield calculations. Typical detection limits are in the range of 30–40 ppb for REE, Sr, Zr, Hf and Y; 200 ppb for V and Sc; 4–6 ppm for Co, Cu, Zn.

4. Results and discussion

4.1. Petrography

The xenolith collection of sixty samples from Tres Lagos (sample prefixed by TL) comprises spinel lherzolites (52%), harzburgites (30%), dunites (11%), websterites (6%) and few clinopyroxenites (Fig. 2). The contacts between xenoliths and the host rocks are generally sharp. Websterites and clinopyroxenites are not included to this study as they are the subject of ongoing investigation. Xenoliths are randomly distributed throughout the host rocks.

The dominant texture, after Mercier and Nicolas (1975), is porphyroclastic transitional to mosaic (50%, Fig. 3a) followed by equigranular mosaic (27%), protogranular (12%) and protogranular transitional to porphyroclastic (11%), documenting mild to strong tectonization (Fig. 3b) in the lithospheric mantle.

The coarse-grained, anhedral olivines (maximum size of 4 mm) are generally strained and kinked and very rarely contain small rounded sulfide and pyroxene inclusions. The small olivine neoblasts in the xenoliths with porphyroclastic, equigranular and transitional textures are strain-free and show straight grain boundaries. Orthopyroxenes carry exsolutions of clinopyroxenes and vice versa, restricted to the core of the grains. Both phases are strained but to a lesser extent than the large olivines. Both orthopyroxene and clinopyroxene carry thin exsolution rods of spinel.

Brown spinels are present in all textural types forming anhedral grains and small interstitial grains, occasionally developing pyroxene-Cr-spinel symplectitic textures. Occasionally light brown glass is present constituting veinlets (50 to 70 μm wide) and patches (average size of 400 × 500 μm, maximum size 1 mm × 600 μm), located interstitially to primary phases (olivine and/or orthopyroxene and/or clinopyroxene and/or spinel) and along fractures. Very thin veinlets (10 μm wide) of sulfides (Fe, Ni and Cu) are present along grain boundaries, in fractures in silicates and spinels and in glassy patches.

4.2. Mineral chemistry

4.2.1. Major elements

Representative analyses of selected main mineral constituents along with rock and textural types of xenoliths from Tres Lagos, as well as mineral end-member calculations, are given in Tables 1a, b, c, d. There is no compositional variation between core and rim in minerals.

Olivine Fo content (Table 1a) ranges between 90 and 91 mol% for harzburgites and lherzolites; in dunites, the Fo mean value is 92 mol%. CaO contents are low (0.02 to 0.06 wt.%) and NiO contents are in the range 0.37–0.42 wt. %. Orthopyroxene average compositions (Table 1b) are in the range $En_{88–90}$ $Wo_{4–1}$ $Fs_{8–9}$ in harzburgites and $En_{90–91}$ Wo_1 $Fs_{9–8}$ in lherzolites. Minor element contents of orthopyroxene vary widely: TiO_2 from 0.05 wt.% to

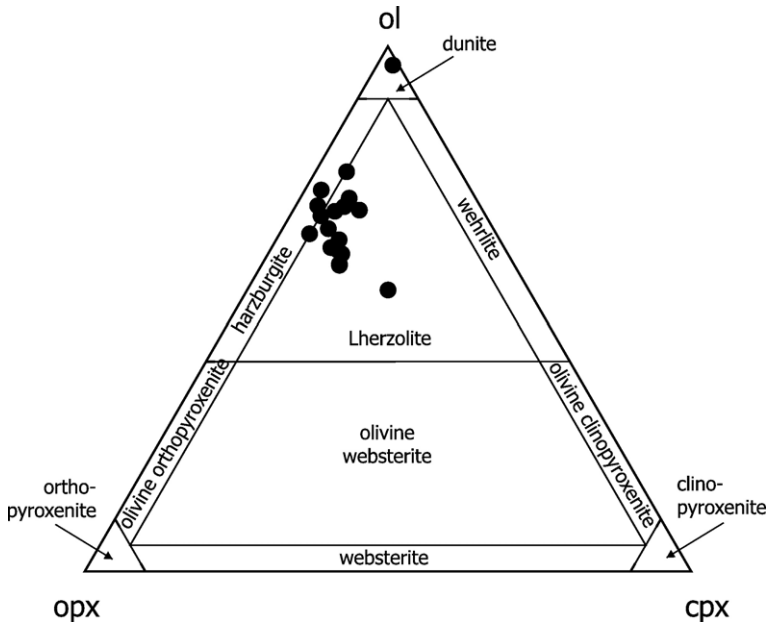

Fig. 2. Rock types identified in the Tres Lagos xenolith collection based on modal mineral abundance.

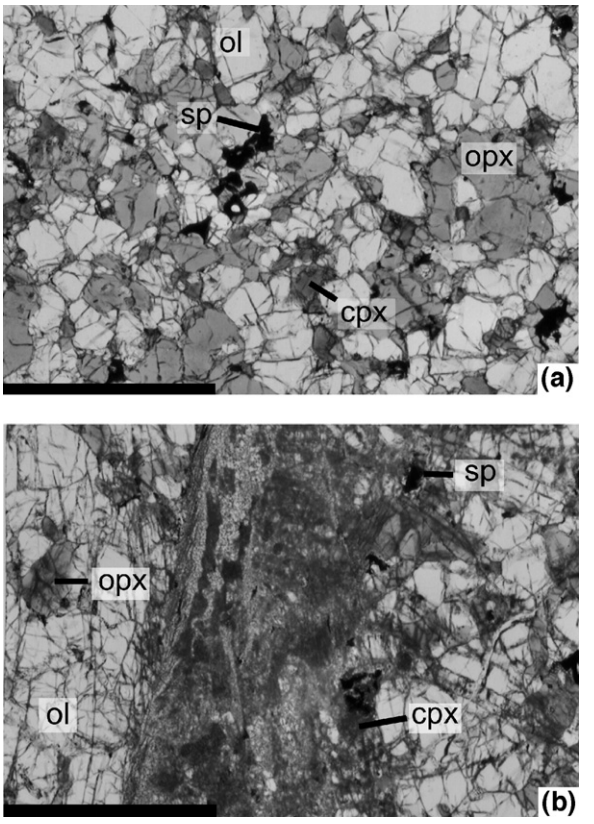

Fig. 3. (a): Porphyroclastic to equigranular spinel harzburgite, b) spinel lherzolite with equigranular texture and highly tectonized zones. Ol: Olivine, opx: orthopyroxene, cpx: clinopyroxene, sp: spinel. Scale bar 1 cm.

0.09 wt.%, Al_2O_3 from 2.78 wt.% to 3.93 wt.%, Cr_2O_3 from 0.28 wt.% to 0.53 wt.% and CaO from 0.38 wt.% to 2.26 wt.%.

Clinopyroxene mean compositions (Table 1c) are En_{49} Wo_{47} Fs_4 in harzburgites, $En_{48–50}$ $Wo_{48–46}$ Fs_4 in lherzolites and En_{50} Wo_{47} Fs_3 in dunites. Clinopyroxenes in lherzolite and harzburgite xenoliths from Tres Lagos display also a wide range in the contents of TiO_2 (0.14–0.53 wt.%), Cr_2O_3 (0.75–1.21 wt.%), Na_2O (0.34–1.57) and a considerable range in Al_2O_3 (2.73–6.54 wt.%). In clinopyroxenes from dunites, the contents of Al_2O_3 (1.39 wt.%) are lower and that of Cr_2O_3 (1.36 wt.%) higher than those observed in the harzburgites and lherzolites. Some of these elements display a rough positive correlation, e.g., Na_2O vs. Al_2O_3 and TiO_2 vs. Al_2O_3 (not shown), while negative correlations are exemplified by mg# vs. TiO_2 and mg# vs. Al_2O_3 (Fig. 4a, b).

The mg# and cr# for spinels (Table 1d) are in the range 74–77 and 16–20 in harzburgites, 74–79 and 12–

Table 1a
Representative olivine microprobe analyses (wt.%)

Sample	TL-101	TL-102	TL-103	TL-104	TL-105	TL-106	TL-107	TL-109	TL-110	TL-111	TL-112	TL-113	TL-114	TL-116	TL-117	TL-119	TL-120	TL-124	TL-133
Rock Type	1	2	2	2	1	1	1	1	1	1	1	1	1	1	1	1	1	1	3
Texture	PtM	PtM	PtM	PtM	M	PtM	PtM	PtM	PtM	PtM	PtM	P	PtM	M	PtM	PtM	PrtP	P	PrtM
SiO2	41.12	40.84	40.32	41.19	40.15	41.29	40.18	41.22	41.34	40.30	40.87	41.10	40.46	41.17	41.11	41.06	41.21	41.16	41.37
Al2O3	0.01	bdl	0.01	0.01	0.01	0.01	0.01	0.04	0.01	0.01	0.01	0.03	0.01	0.01	0.01	0.01	0.01	0.01	0.01
Cr2O3	0.01	0.01	0.01	0.01	0.02	0.01	0.01	0.03	0.01	0.02	0.03	0.03	0.01	0.03	0.01	0.01	0.01	0.03	0.02
FeO[a]	9.13	9.30	8.96	8.74	8.93	8.99	8.89	9.27	8.70	9.42	9.48	8.68	9.10	8.77	9.22	8.60	9.60	8.84	7.75
MnO	0.13	0.14	0.14	0.12	0.14	0.14	0.13	0.14	0.13	0.15	0.14	0.13	0.15	0.14	0.14	0.13	0.13	0.15	0.11
MgO	50.15	49.65	49.86	50.57	50.14	50.47	49.95	50.18	50.50	49.84	50.13	50.73	50.19	50.28	50.33	50.38	50.15	50.83	51.67
CaO	0.06	0.04	0.05	0.03	0.03	0.04	0.04	0.04	0.04	0.04	0.04	0.11	0.04	0.11	0.02	0.05	0.04	0.04	0.05
NiO	0.40	0.39	0.38	0.40	0.42	0.42	0.39	0.37	0.40	0.39	0.38	0.39	0.38	0.40	0.38	0.41	0.38	0.42	0.37
Total	101.02	100.38	99.74	101.08	99.85	101.40	99.60	101.31	101.14	100.18	101.10	101.23	100.35	100.93	101.24	100.67	101.54	101.48	101.38
Fo[b]	90.73	90.49	90.84	91.16	90.92	90.92	90.92	90.61	91.19	90.41	90.41	91.24	90.77	91.09	90.68	91.26	90.30	91.11	92.24

Rock type: 1 — spinel lherzolite; 2 — spinel harzburgite; 3 — dunite. Texture: PtM — porphyroclastic to mosaic; M — mosaic; P — porphyroclastic; PrtP — protogranular to porphyroclastic; PrtM — protogranular to mosaic.

[a] Fe total as FeO.

[b] Fo: forsterite; bdl: below detection limit.

Table 1b
Representative orthopyroxene microprobe analyses (wt.%)

Sample	TL-101	TL-102	TL-103	TL-104	TL-105	TL-106	TL-107	TL-109	TL-110	TL-111	TL-112	TL-113	TL-114	TL-116	TL-117	TL-119	TL-120	TL-124
Rock Type	1	2	2	2	1	1	1	1	1	1	1	1	1	1	1	1	1	1
Texture	PtM	PtM	PtM	PtM	M	PtM	PtM	PtM	PtM	PtM	PtM	P	PtM	M	PtM	PtM	PrtP	P
SiO2	55.80	55.62	54.92	55.58	55.10	56.23	55.40	56.01	56.30	55.40	55.80	56.10	55.50	55.90	56.20	55.80	53.77	56.31
TiO2	0.09	0.07	0.08	0.09	0.08	0.07	0.07	0.06	0.08	0.08	0.08	0.08	0.08	0.05	0.06	0.08	0.09	0.07
Al2O3	2.99	2.89	3.45	3.62	3.06	3.30	3.29	3.30	2.84	3.63	3.24	3.11	3.42	3.19	2.78	3.30	3.71	3.20
Cr2O3	0.41	0.35	0.38	0.53	0.41	0.42	0.31	0.53	0.46	0.33	0.28	0.28	0.43	0.51	0.42	0.39	0.36	0.38
FeO[a]	5.94	6.01	5.88	5.38	5.76	5.94	5.69	6.08	5.70	6.11	6.08	5.67	5.84	5.73	6.03	5.54	6.44	5.62
MnO	0.15	0.16	0.15	0.14	0.16	0.15	0.16	0.16	0.13	0.16	0.16	0.14	0.16	0.14	0.15	0.14	0.13	0.15
MgO	34.20	34.21	34.21	32.97	34.50	34.51	34.40	34.57	34.80	34.30	34.60	34.90	34.10	34.20	34.80	34.50	36.20	34.82
CaO	0.49	0.38	0.47	2.26	0.40	0.50	0.40	0.57	0.39	0.38	0.39	0.45	0.69	0.56	0.38	0.43	0.44	0.47
NiO	0.10	0.10	0.09	0.09	0.09	0.08	0.08	0.09	0.07	0.09	0.09	0.09	0.08	0.10	0.08	0.09	0.11	0.09
Na2O	0.03	0.02	0.03	0.10	0.03	0.01	0.03	0.01	0.03	0.02	0.03	0.04	0.05	0.10	0.01	0.04	0.04	0.05
K2O	0.01	bdl	bdl	bdl	bdl	0.01	bdl	bdl	0.01	bdl	bdl	bdl	bdl	bdl	bdl	bdl	bdl	bdl
Total	100.21	99.81	99.66	100.80	99.59	101.22	99.83	101.38	100.81	100.50	100.75	100.86	100.35	100.48	100.91	100.31	101.29	101.16
En	90.1	90.1	90.2	87.5	90.5	90.2	90.6	89.8	90.7	90.0	90.2	90.7	89.8	90.3	90.3	90.8	90.0	90.7
Fs	9.0	9.2	8.9	8.2	8.7	8.9	8.6	9.1	8.5	9.3	9.1	8.5	8.9	8.7	9.0	8.4	9.2	8.4
Wo	0.9	0.7	0.9	4.3	0.8	0.9	0.8	1.1	0.7	0.7	0.7	0.8	1.3	1.1	0.7	0.8	0.8	0.9

Rock type and texture as in Table 1a.

[a] Fe total as FeO; bdl: below detection limit; En: enstatite; Fs: ferrosilite; Wo: wollastonite.

25 in lherzolites, respectively. In dunites, the average values of these parameters are 57 and 72, respectively.

4.3. Clinopyroxene minor and trace elements

Minor and trace element analyses of 18 clinopyroxene grains are presented in Table 1c and as Primitive Mantle (PM)-normalized trace element diagrams (Fig 5a, b). According to their trace element abundances, clinopyroxenes can be distinguished into unmetasomatized and metasomatized clinopyroxenes. Unmetasomatized clinopyroxenes, which comprise the majority of the studied samples, exhibit convex-upward trace element patterns with negative Ti, Zr and Sr anomalies (Fig. 5a). Heavy REE contents are typically around 2.5–5 × PM, whereas the La/Yb ratios vary from 0.1 to 0.7. Metasomatized clinopyroxenes have HREE contents typically below 2 × PM. Their La/Yb ratios range from 1.2 to 7.5 and the PM-normalized patterns exhibit strong to moderate LREE enrichments (Fig. 5b). Spidergrams show moderate to strong Ti anomalies, weak positive to negative Zr anomalies and weak to strong negative Sr anomalies.

Both, unmetasomatized and metasomatized clinopyroxenes display distinct positive linear trends on a Sr vs. La diagram (Fig. 6a). The Sr/La ratios in unmetasomatized clinopyroxenes are higher than that of the undepleted mantle (Sr/La of PM ~30), consistent with depletion after various degrees of partial melting. In the metasomatized clinopyroxenes the Sr/La ratios are lower than that of the undepleted mantle which is consistent with metasomatic processes affecting these samples. Zirconium abundances in clinopyroxenes are also coupled with the LREE depletions (Fig. 6b). In unmetasomatized samples, with exception of samples TL-120 and TL-135, Zr correlates broadly positive with La, a trend that, though weak, is also consistent with partial melting processes taking place. In contrast, the La enrichments in the metasomatized samples do not show any correlation with Zr.

4.4. Bulk rock chemistry

4.4.1. Major elements

Tres Lagos peridotites display a restricted compositional range in major element abundances indicating that they experienced moderate to strong depletion in basaltic components (Table 2, Fig. 7a, b). The Al_2O_3 and CaO contents vary from 0.58 to 2.74 and from 0.46 to 2.94, respectively. The linear trends in the Al_2O_3 vs. MgO and CaO vs. Al_2O_3 correlation diagrams (Fig. 7a, b) are in agreement with the peridotites being derived from the same fertile source via different degrees of partial melting. Similar trends, not shown here, were found between MgO and various incompatible trace elements. It is remarkable that among the collected samples no fertile peridotites were found. Compared to the Pali Aike spinel peridotites (Stern et al., 1999), a volcanic field located ca. 300 km south of Tres Lagos, they show a slight but systematic enrichment in CaO contents (Fig. 7a, b).

4.4.2. Rare earth elements

According to the bulk-rock REE abundances in the Tres Lagos peridotites, they can be divided into four groups: group 1 comprises the dunites, which have PM-normalized REE abundance patterns (Fig. 8a), showing a strong LREE enrichment [(La_n/Sm_n)=6.2–12.6] and a strong HREE depletion [(Tb_n/Yb_n)=0.20–0.25]. The REE pattern of dunite TL-134 reveals a complex history. The HREE appear to be undisturbed whereas the MREE are enriched relative to HREE [(Sm_n/Ho_n)=5–6.5], indicating that this rock has been affected by metasomatism. The LREE show an inverse spoon-like shape and are enriched relative to MREE (La/Sm 8–12.6), suggesting that the latest event was a distinct metasomatic event, which intensely affected only the LREE.

In group 2, which encompasses lherzolites and harzburgites, the REE patterns reveal partial melting processes and depletion of basaltic components (Fig. 8b). The LREE are depleted relative to HREE [(La_n/Yb_n)=0.61–1.48] even though they show a slight upward trend, which is the result of a late-stage metasomatism due to the introduction of fluids and/or small amounts of host lava.

Group 3, which also comprises lherzolites and harzburgites, is enriched in LREE relative to HREE [(La_n/Yb_n)=4.2–4.9 and (La_n/Sm_n)=3.4–5.7)], suggesting that these rocks have been more strongly affected by metasomatic fluids/melts than those of group 2 (Fig. 8c).

In group 4 the REE abundance patterns have a U-shape, with positive to flat middle to heavy REE slopes, and enriched LREE, that cannot be explained by simple melting and requires, like in the case of group 3, secondary enrichments (Fig. 8d).

4.4.3. Sr–Nd isotopes

Whole rock powders from eight representative xenolith samples have been analyzed for Sr–Nd isotopes (Table 3). Samples were not leached before analysis. The $^{143}Nd/^{144}Nd$ ratios vary from 0.512733 to 0.513118 and the $^{87}Sr/^{86}Sr$ ratios from 0.70440 to 0.70599. All samples plot (Fig. 9) between HIMU, PREMA and BSE and above the field of Meseta Central basalts (MCB) (Gorring and

Table 1c
Representative clinopyroxene major element microprobe analyses (wt.%) and LA-ICP-MS trace elements (ppm)

Sample	TL-101	TL-102	TL-103	TL-104	TL-105	TL-106	TL-107	TL-109	TL-110	TL-111
Rock Type	1	2	2	2	1	1	1	1	1	1
Texture	PtM	PtM	PtM	PtM	M	PtM	PtM	PtM	PtM	PtM
SiO2	52.25	52.26	52.23	52.80	51.99	52.69	51.63	53.16	52.38	51.78
TiO2	0.39	0.30	0.33	0.22	0.35	0.23	0.37	0.23	0.40	0.33
Al2O3	4.76	4.18	4.42	3.89	4.00	4.03	5.20	2.99	4.23	4.96
Cr2O3	0.93	0.82	0.86	0.76	0.84	0.82	0.81	0.70	1.16	0.70
FeO*	2.18	2.24	2.15	2.12	2.10	2.16	2.15	2.01	2.07	2.19
MnO	0.07	0.07	0.08	0.08	0.07	0.07	0.07	0.07	0.07	0.07
MgO	16.00	16.65	16.35	16.93	16.57	17.38	16.11	17.31	16.35	16.15
CaO	22.57	22.70	22.23	22.42	22.80	22.88	22.38	23.74	22.74	22.77
NiO	0.04	0.04	0.04	0.05	0.04	0.05	0.04	0.05	0.03	0.02
Na2O	0.97	0.78	0.99	0.83	0.81	0.54	0.95	0.50	0.90	0.88
K2O	bdl	bdl	0.01	bdl	0.01	0.01	bdl	bdl	bdl	bdl
Total	100.16	100.04	99.69	100.10	99.58	100.86	99.71	100.76	100.33	99.85
En	47.8	48.6	48.7	49.4	48.5	49.6	48.2	48.7	48.2	47.8
Fs	3.8	3.8	3.7	3.6	3.5	3.6	3.7	3.3	3.5	3.8
Wo	48.5	47.6	47.6	47.0	48.0	46.9	48.1	48.0	48.2	48.4
Sc	66.4	na	78.9	68.2	69.1	71.9	76.3	66.7	na	70.5
Cr	6353	na	6134	5818	5557	5495	5227	5792	na	5308
Co	26.6	na	20.4	22.3	24.9	24.8	22.1	30.5	na	27.9
Ni	420	na	316	352	403	361	358	435	na	405
Zn	49.0	na	18.1	23.1	24.0	27.2	25.6	33.3	na	43.8
Cu	4.31	na	5.76	8.02	15.1	9.40	7.04	8.69	na	6.33
V	268	na	263	256	278	268	258	244	na	268
Sr	17.91	na	20.1	7.17	13.1	9.79	16.0	18.2	na	9.37
Y	11.8	na	12.8	12.0	16.6	9.02	15.51	8.67	na	13.9
Zr	6.07	na	24.8	5.54	11.6	5.15	11.3	4.32	na	6.12
La	0.225	na	0.280	0.155	0.225	0.253	0.213	0.315	na	0.200
Ce	0.745	na	1.595	0.580	0.905	0.860	0.848	1.075	na	0.885
Pr	0.215	na	0.363	0.150	0.258	0.213	0.263	0.260	na	0.170
Nd	1.665	na	2.465	1.200	2.160	1.260	2.108	1.290	na	1.250
Sm	0.825	na	1.170	0.738	1.460	0.723	0.953	0.000	na	0.990
Eu	0.340	na	0.428	0.395	0.605	0.333	0.503	0.000	na	0.395
Gd	1.510	na	1.578	1.390	2.238	1.180	2.123	1.360	na	1.360
Tb	0.275	na	0.298	0.285	0.535	0.250	0.398	0.180	na	0.340
Dy	1.935	na	2.008	1.995	2.965	1.717	2.530	1.740	na	2.245
Ho	0.455	na	0.473	0.505	0.768	0.400	0.660	0.335	na	0.560
Er	1.385	na	1.418	1.415	1.875	1.097	1.713	0.860	na	1.450
Tm	0.185	na	0.238	0.238	0.323	0.150	0.285	0.145	na	0.245
Yb	1.355	na	1.523	1.485	2.218	1.177	1.693	1.050	na	1.540
Lu	0.175	na	0.223	0.225	0.293	0.160	0.223	0.115	na	0.215
Hf	0.440	na	0.775	0.353	0.568	0.453	0.558	0.700	na	0.940

Rock type and texture as in Table 1a.*Fe total as FeO; ** Fo: forsterite; bdl: below detection limit; na: not analyzed.

Kay, 2001). Sample TL-133, a strongly metasomatized dunite (Fig. 9), shows high Sr- and the lowest Nd-isotopic ratios among the analyzed samples. Samples TL-101, TL-103-TL-109 and TL-116 form a group that plots close to the MCB. These samples have been affected by metasomatic processes and exhibit U-shaped whole rock trace element patterns (Fig. 8d).

Samples TL-104 and TL-111 have the highest Nd-isotopic ratios (0.513043 and 0.513118, respectively) and relatively high Sr-isotope ratios (0.705506 and 0.705090, respectively). The corresponding whole rock REE patterns exhibit LREE-depletion in respect to HREE and their clinopyroxene REE patterns reflect whole rock patterns (Fig. 8b) arguing against any metasomatic influence.

TL-112	TL-113	TL-114	TL-116	TL-117	TL-119	TL-120	TL-124	TL-133
1	1	1	1	1	1	1	1	3
PtM	P	PtM	M	PtM	PtM	PrtP	P	PrtM
51.76	52.11	51.97	52.49	53.12	51.97	52.26	52.38	54.74
0.47	0.42	0.38	0.24	0.19	0.48	0.49	0.42	0.09
5.61	5.71	5.35	5.06	2.76	5.66	5.74	5.48	1.44
0.80	0.94	1.01	1.20	0.64	1.10	0.79	1.12	1.30
2.27	2.38	2.13	2.13	2.08	2.04	2.25	2.11	1.93
0.08	0.08	0.08	0.08	0.07	0.08	0.07	0.07	0.04
15.81	16.27	15.79	15.55	17.47	15.37	15.66	15.80	17.16
22.29	21.13	22.06	21.53	22.32	21.56	22.26	22.10	22.74
0.06	0.04	0.05	0.04	0.03	0.03	0.03	0.05	0.04
1.09	1.22	1.22	1.49	0.40	1.36	1.26	1.28	1.23
0.01	bdl	bdl	bdl	bdl	bdl	0.01	bdl	bdl
100.25	100.30	100.04	99.81	99.08	99.65	100.82	100.81	100.71
47.7	49.5	48.0	48.2	50.3	48.0	47.5	48.0	49.6
4.0	4.2	3.8	3.8	3.5	3.7	4.0	3.7	3.2
48.3	46.3	48.2	48.0	46.2	48.3	48.5	48.3	47.2
66.9	71.1	69.6	60.7	80.6	71.6	na	79.0	143.1
4225	5998	6839	7366	6249	6589	na	5230	7054
19.8	23.9	25.3	21.3	33.4	21.2	na	24.5	20.7
265	337	360	375	463	361	na	31	287
13	32.0	41.5	24.7	19.5	16.855	na	23.9	12.2
10.7	9.93	6.25	9.26	15.7	12.4	na	4.90	9.60
280	277	260	241	236	267	na	300	135
17.6	16.7	20.5	26.4	6.18	30.3	na	14.9	31.5
12.9	16.7	11.8	6.16	8.00	15.2	na	16.1	5.39
9.86	16.1	11.1	6.87	18.9	26.7	na	11.4	12.1
0.340	0.253	0.565	2.105	0.835	0.355	na	0.249	5.22
1.280	1.133	2.465	4.120	2.295	1.988	na	1.136	8.350
0.337	0.356	0.410	0.465	0.260	0.515	na	0.316	0.720
2.173	2.644	2.450	1.940	1.630	3.248	na	2.407	2.560
1.003	1.588	1.220	0.940	0.580	1.698	na	1.389	0.660
0.460	0.747	0.490	0.280	0.235	0.583	na	0.615	0.210
2.000	2.490	1.920	0.905	1.025	2.138	na	2.276	0.890
0.383	0.528	0.370	0.165	0.175	0.383	na	0.451	0.145
2.723	3.474	2.650	1.085	1.250	2.825	na	2.919	0.905
0.580	0.857	0.590	0.285	0.320	0.633	na	0.715	0.230
1.757	2.206	1.635	0.800	1.045	1.730	na	2.045	0.730
0.233	0.298	0.225	0.140	0.150	0.245	na	0.270	0.120
1.727	1.849	1.910	0.920	0.700	1.438	na	1.892	0.700
0.263	0.284	0.255	0.120	0.105	0.215	na	0.296	0.110
0.610	0.720	0.720	0.295	0.860	1.150	na	0.650	0.480

These samples plot away from the MCB-field towards very high Sr- and Nd-isotopic ratios.

4.4.4. PT-conditions

Estimates of equilibrium conditions for Tres Lagos xenoliths are based on mineral core compositions and the two-pyroxene thermometer of Brey and Köhler (1990). Calculated equilibrium temperatures vary in the range 728 to 1040 °C.

Because pressure estimates with the geobarometer of Köhler and Brey (1990) gave unreasonable pressures, the empirical geobarometer of Mercier et al. (1984) was used. At Tres Lagos, the equilibration pressure varies between 10 and 17 kbar, reflecting a rather cold environment and

Table 1d
Representative spinel microprobe analyses (wt.%)

Sample	TL-101	TL-102	TL-103	TL-104	TL-105	TL-106	TL-107	TL-109	TL-110	TL-111	TL-112	TL-113	TL-114	TL-116	TL-117	TL-119	TL-120	TL-124	TL-133
Rock Type	1	2	2	2	1	1	1	1	1	1	1	1	1	1	1	1	1	1	3
Texture	PtM	PtM	PtM	PtM	M	PtM	PtM	PtM	PtM	PtM	PtM	P	PtM	M	PtM	PtM	PrtP	P	PrtM
SiO2	0.03	0.02	0.03	0.03	0.03	0.02	0.03	0.02	0.03	0.03	0.04	0.05	0.02	0.03	0.03	0.02	0.03	0.03	0.03
TiO2	0.10	0.09	0.05	0.05	0.10	0.05	0.05	0.07	0.13	0.04	0.07	0.06	0.08	0.01	0.07	0.07	0.07	0.07	0.32
Al2O3	50.91	48.72	52.84	50.93	48.80	49.82	56.72	46.39	44.39	56.93	56.61	55.02	52.61	49.37	45.15	52.17	57.01	51.82	13.57
Cr2O3	16.52	19.11	16.03	17.12	19.83	18.13	12.46	22.48	22.83	11.69	11.52	13.15	16.16	19.00	22.90	15.76	11.06	16.56	53.61
FeO*	10.86	11.89	10.66	10.87	11.34	11.06	9.62	12.48	12.25	10.65	10.39	9.81	10.89	10.00	12.98	10.26	10.48	10.37	17.83
MnO	0.09	0.09	0.07	0.08	0.10	0.09	0.08	0.10	0.08	0.11	0.07	0.06	0.09	0.06	0.09	0.07	0.09	0.07	0.13
MgO	20.05	19.18	19.52	20.23	18.90	19.87	20.64	18.43	18.86	20.21	20.76	21.24	19.63	20.62	18.24	20.53	20.84	20.42	13.45
CaO	0.01	bdl	bdl	bdl	bdl	bdl	bdl	bdl	0.01	bdl	0.01	bdl	0.02	0.01	0.01	0.00	0.00	0.01	0.01
NiO	0.33	0.27	0.30	0.33	0.28	0.30	0.37	0.25	0.28	0.35	0.34	0.34	0.33	0.31	0.27	0.34	0.38	0.35	0.11
Na2O	bdl	0.01	bdl	0.01	0.01	bdl	bdl	0.01	0.01	0.01	0.01	bdl	0.01	0.01	0.01	0.01	0.01	0.01	0.01
K2O	bdl	0.01	0.01	bdl	0.01	0.01	bdl	bdl	bdl	bdl	bdl	0.01	bdl	bdl	0.01	bdl	bdl	0.01	0.01
Total	98.90	99.39	99.51	99.65	99.40	99.35	99.97	100.23	98.87	100.02	99.82	99.74	99.84	99.42	99.76	99.23	99.97	99.72	99.08
mg#	76.7	74.2	76.5	76.8	74.8	76.2	79.3	72.5	73.3	77.2	78.1	79.4	76.3	78.6	71.5	78.1	78.0	77.8	57.3
cr#	17.9	20.8	16.9	18.4	21.4	19.6	12.8	24.5	25.7	12.1	12.0	13.8	17.1	20.5	25.4	16.9	11.5	17.7	72.6

Rock type and texture as in Table 1a.
* Fe total as FeO; bdl: below detection limit; mg#: (Mg/Mg+Fe)*100; cr#: (Cr/Cr+Al)*100.

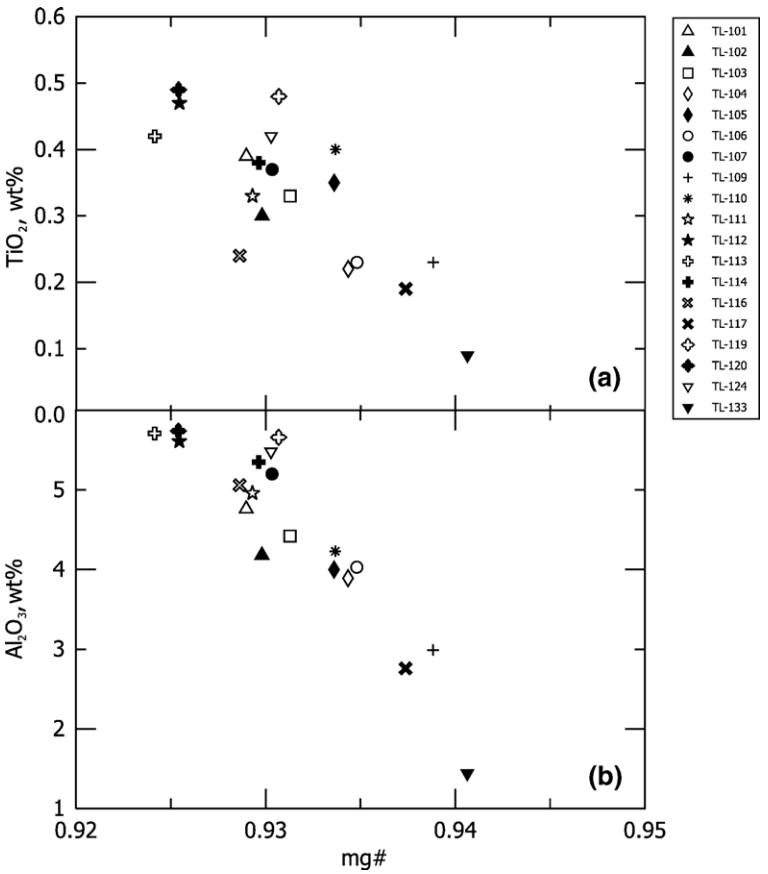

Fig. 4. Variation of cpx TiO_2 and Al_2O_3 against mg# for Tres Lagos xenoliths, a) cpx TiO_2 (wt.%) vs. mg#, b) cpx Al_2O_3 (wt.%) vs. mg#.

shallow depths in comparison with xenoliths from other Patagonian localities (Bjerg et al., 2005).

4.5. Partial melting processes

The lack of spinel peridotites with a primitive chemical composition is a common characteristic of the Patagonian localities (Rivalenti et al., 2004; Bjerg et al., 2005) and the spinel peridotites from Tres Lagos are no exception. Only garnet-bearing xenoliths from Pali Aike have compositions close to the primitive mantle (Stern et al., 1999; Bjerg et al., 2005). The MgO content varies from about 40 to 50 wt.%. This depletion signature is confirmed by the negative correlation of bulk Al_2O_3 with MgO and cpx mg# with TiO_2 and Al_2O_3 (Fig. 4 a, b). These trends demonstrate a partial melting control on the compositions of these rocks due to the extraction of basaltic melts from a former fertile mantle (Frey et al., 1985). The Tres Lagos spinel peridotites are richer in CaO at similar Al_2O_3 contents compared to the Pali Aike xenoliths (Fig. 7a, b). This evidence could be taken as an indicator for carbonatite metasomatism, which is clearly evident at Gobernador Gregores locality (Gorring and Kay, 2000), located 130 km NE of Tres Lagos. However, other than the slightly elevated CaO/Al_2O_3 ratio, there is no additional evidence that supports carbonatite metasomatism. Modal heterogeneity is also common in orogenic peridotites and other mantle xenoliths. Niu and Batiza (1991) modeled the effects of melt extraction on the Ca/Al ratio, taking also into account possible effects of modal heterogeneity. In Fig. 10 (adapted from O'Neill and Palme, 1998) the Tres Lagos samples clearly demonstrate sample heterogeneity as the trend follows the vector that shows the direction of increasing Ca/Al ratio due to clinopyroxene modal heterogeneity. Further evidence for partial melting control is manifested in the clinopyroxene REE abundance. However, almost half of the studied xenoliths have whole rock REE abundance patterns enriched in LREE and MREE over HREE. Hydrous phases like amphibole and/or phlogopite were not found in the investigated samples. Therefore the LREE–MREE enrichment can be ascribed either to cryptic metasomatism or to intergranular fluids/melts. As clinopyroxene, the major repository for trace elements in spinel peridotites,

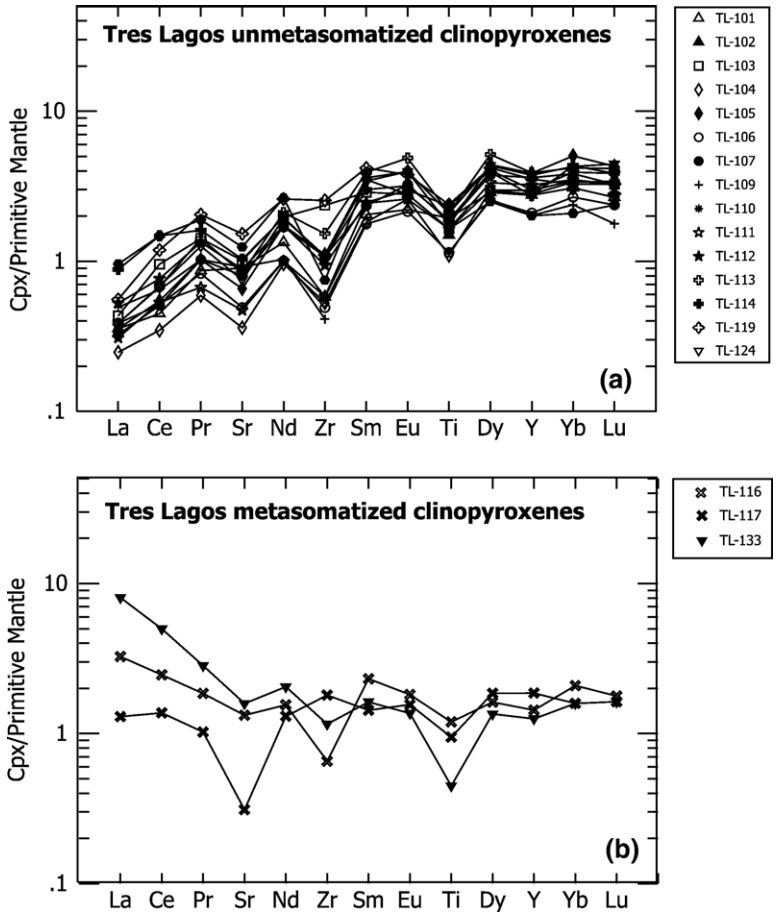

Fig. 5. LA-ICP-MS PM-normalized clinopyroxene REE concentration patterns of selected Tres Lagos xenoliths, a) non-metasomatized clinopyroxenes, b) metasomatized clinopyroxenes. Primitive Mantle (PM)-normalizing values from McDonough and Sun (1995).

shows a depletion of LREE with respect to HREE, cryptic metasomatism can be excluded as possible LREE enrichment mechanism in all samples except TL-116, TL-117 and TL-133. The other half of the studied samples, that is group 2, exhibits whole rock REE patterns typical for residues after extraction of basaltic components due to partial melting. Also, the REE abundances in clinopyroxene reflects those in the whole rock.

4.5.1. Modelling

The clinopyroxene trace element patterns (Fig. 5a, b) suggest that the Tres Lagos xenoliths are residues after different degrees of partial melting of a primitive mantle, which have been affected to some extent by metasomatism. Melting trends recorded in the clinopyroxenes cannot be modeled by applying the techniques developed by Johnson et al. (1990) and Norman (1998) as the LREE have La/Nd ratios higher than those that could be predicted by batch melting and lower than those corresponding to fractional melting processes. Based on the fact that at the Pali Aike volcanic province, located 300 km south of Tres Lagos, garnet-bearing xenoliths occur (Stern et al., 1990, 1999, Kempton et al., 1999a, 1999b, Bjerg et al., 2005), a two-stage model of partial melting has been proposed. Possibly, the Tres Lagos peridotites, some of which carry characteristic pyroxene-Cr-spinel symplectites, have experienced partial melting first in the garnet peridotite field and subsequently also in the spinel peridotite stability field. The transition from the garnet peridotite to the spinel peridotite field could have taken place in a scenario of rising mantle plume(s) in an extensional tectonic setting, which is supported by the anomalous high geotherm beneath Patagonia and the predominance of tectonized textural types (Bjerg et al., 2005).

REE and Zr can be easily modeled if the residue left after 2% batch melting of a primitive mantle in the garnet peridotite field (with modal proportions taken from

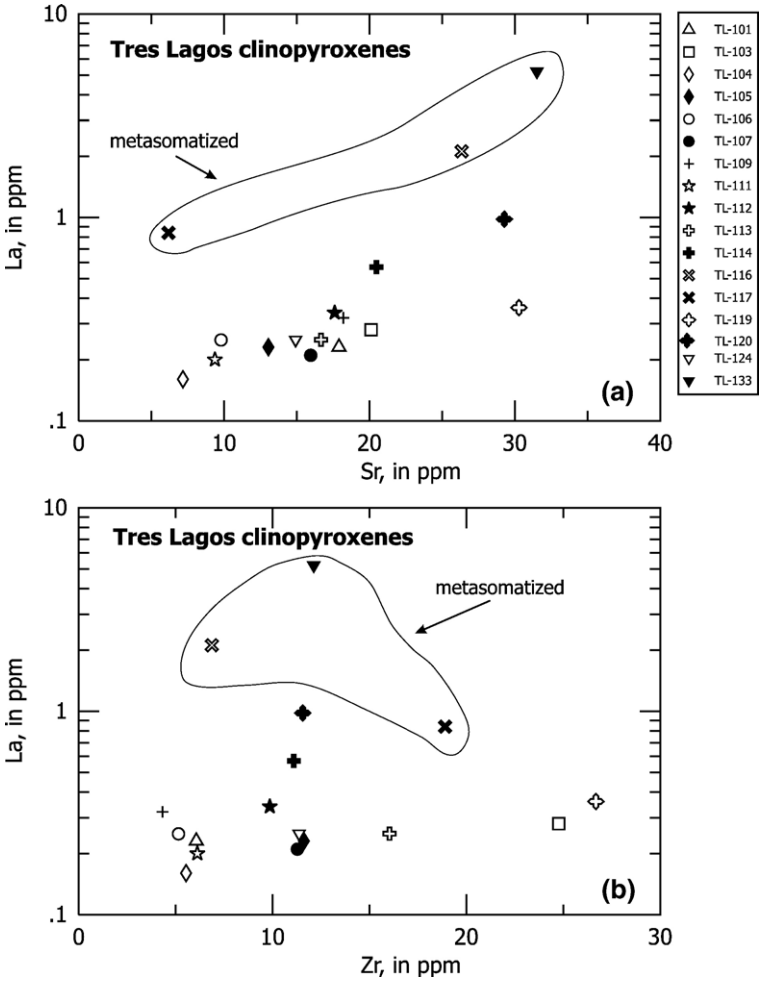

Fig. 6. Correlation between Sr, Zr vs. La (ppm) for clinopyroxenes from Tres Lagos, a) non-metasomatized and metasomatized clinopyroxenes, b) coupling between LREE and Zr abundances.

Johnson et al., 1990) is the melting source for the studied samples in the spinel peridotite field. The method, described by Norman (1998), reveals that the Tres Lagos xenoliths, after their initial 2% partial melting in the garnet peridotite field, have experienced 2–8% partial melting in the spinel peridotite field (Fig. 11). The observed pronounced negative Ti anomaly cannot be predicted by applying common mineral-melt partition coefficients. Norman (1998) suggested that Ti depletion can be modeled if the mineral-melt partition coefficient is lower than those referred in the literature (e.g. Johnson et al., 1990) by a factor 2–3. Xu et al. (2000), using lower Kd values modeled the clinopyroxene Ti depletion in peridotites from Southeastern China. They argued that the Ti Kd's between pyroxenes and basaltic melts were determined experimentally using augitic pyroxenes, in which Al is distributed equally between Al^{IV} and Al^{VI} sites, whereas in diopside it is mainly located in the octahedral position. Titanium can substitute Al^{IV} in augite phenocrysts and therefore the partition coefficient for Ti will be higher than that for diopsides (Xu et al., 2000). Fig. 12 shows nicely the dependency of Ti_{Kd} from Al in the tetrahedral position.

Another peculiarity of the Tres Lagos xenoliths is their strong depletion in Sr in clinopyroxene. The partitioning behavior of Sr in melting processes is similar to that of Ce and Nd. Green et al. (2000) argue that these anomalies can be generated by changing the P–T melting conditions without the necessity to invoke fractionation processes or metasomatism. Taking into account the above arguments and using for Sr a distribution coefficient of 0.066 as given by Green et al. (2000), the negative Sr anomaly observed in the Tres Lagos samples can be modeled by 2 to 8% batch melting (Fig. 11).

Table 2
Bulk rock analyses of selected samples

Sample	TL-101	TL-102	TL-103	TL-104	TL-105	TL106	TL-107	TL-108	TL-109	TL-110	TL-111	TL-112	TL-113	TL-114
Rock Type	1	2	2	2	1	1	1	2	1	1	1	1	1	1
Texture	PtM	PtM	PtM	PtM	M	PtM	PtM	M	PtM	PtM	PtM	PtM	P	PtM
SiO_2 wt.%	43.90	44.70	43.90	45.40	44.80	44.80	45.20	42.30	45.40	44.60	45.00	45.20	44.20	45.00
TiO_2	0.07	0.08	0.06	0.06	0.078	0.06	0.09	0.045	0.06	0.07	0.08	0.094	0.08	0.085
Al_2O_3	1.39	1.76	1.55	2.05	2.52	1.59	2.74	0.58	1.58	1.33	2.58	2.65	1.80	1.97
Fe_2O_3 [a]	9.40	9.50	9.40	8.60	8.80	9.00	8.50	9.50	8.90	8.90	9.10	8.90	8.90	8.60
MnO	0.13	0.13	0.13	0.12	0.13	0.13	0.12	0.13	0.13	0.12	0.13	0.13	0.12	0.12
MgO	44.90	44.00	44.80	43.00	42.00	43.40	40.80	47.70	42.90	44.90	41.40	40.90	43.90	41.90
CaO	1.30	0.95	0.76	1.81	2.33	1.73	2.94	0.46	1.96	0.72	2.65	2.80	1.86	2.47
Na_2O	0.09	0.08	0.08	0.10	0.12	0.08	0.14	0.06	0.11	0.060	0.122	0.116	0.107	0.110
K_2O	0.01	0.01	0.002	<0.001	0.002	0.003	0.008	0.001	0.027	<0.001	0.006	<0.001	0.005	0.005
Total	101.19	101.24	100.69	101.12	100.78	100.82	100.42	100.77	101.09	100.68	101.07	100.74	101.03	100.21
mg#	90.5	90.3	90.5	90.9	90.6	90.6	90.6	90.9	90.6	91.0	90.1	90.2	90.8	90.7
Sc ppm	5.5	6.8	4.6	8	8.1	9.3	11.7	3.1	10.1	5.9	10.1	12.1	9.2	10.4
V	31	40	30	44	47	46	56	15	47	33	50	61	39	51
Cr	1499	1589	1795	2574	2195	2321	2947	1076	2503	2398	2427	2427	1713	2772
Co	113	110	113	102	101	107	97	122	103	110	102	100	107	99
Ni	2468	2187	2374	2258	2223	2316	2120	2700	2238	2317	2161	2136	2380	2207
Zn	50	43	48	42	43	43	48	44	45	46	47	45	42	46
Ga	2	2.3	2.2	2.6	2.5	2.2	3.3	1.8	2.1	2	2.7	3.1	2.3	2.5
Rb	0.7	0.6	0.7	0.5	0.4	0.6	0.6	0.4	0.5	0.5	0.7	0.8	0.3	0.7
Sr	3.8	5.5	3.1	2.4	3.5	2.7	4.3	3.1	3.5	2	3.4	4.1	3.6	4.1
Y	0.8	0.6	0.5	0.5	0.9	0.8	1.3	0.6	0.8	0.4	2.0	1.4	1.1	0.4
Zr	2.3	3.5	1.9	0.6	1.4	0.7	2.6	0.4	1.7	1.3	1.4	2.4	2.4	2.1
La	*0.254*	*0.341*	*0.122*	*0.049*	na	*0.394*	*0.205*	na	*0.192*	na	*0.097*	na	na	na
Ce	*0.670*	*0.840*	*0.239*	*0.124*	na	*0.993*	*0.502*	na	*0.343*	na	*0.154*	na	na	na
Pr	*0.087*	*0.087*	*0.036*	*0.015*	na	*0.130*	*0.076*	na	*0.044*	na	*0.030*	na	na	na
Nd	*0.339*	*0.357*	*0.156*	*0.075*	na	*0.494*	*0.388*	na	*0.198*	na	*0.166*	na	na	na
Sm	*0.077*	*0.099*	*0.055*	*0.034*	na	*0.100*	*0.163*	na	*0.080*	na	*0.091*	na	na	na
Eu	*0.026*	*0.037*	*0.021*	*0.017*	na	*0.033*	*0.066*	na	*0.027*	na	*0.035*	na	na	na
Gd	*0.110*	*0.117*	*0.065*	*0.063*	na	*0.135*	*0.277*	na	*0.110*	na	*0.157*	na	na	na
Tb	*0.023*	*0.019*	*0.015*	*0.014*	na	*0.027*	*0.055*	na	*0.021*	na	*0.032*	na	na	na
Dy	*0.149*	*0.119*	*0.089*	*0.107*	na	*0.179*	*0.381*	na	*0.155*	na	*0.229*	na	na	na
Ho	*0.035*	*0.026*	*0.021*	*0.027*	na	*0.042*	*0.088*	na	*0.037*	na	*0.053*	na	na	na
Er	*0.108*	*0.081*	*0.069*	*0.091*	na	*0.131*	*0.267*	na	*0.114*	na	*0.161*	na	na	na
Tm	*0.017*	*0.013*	*0.013*	*0.014*	na	*0.021*	*0.041*	na	*0.019*	na	*0.024*	na	na	na
Yb	*0.118*	*0.084*	*0.092*	*0.096*	na	*0.140*	*0.264*	na	*0.130*	na	*0.159*	na	na	na
Lu	*0.019*	*0.014*	*0.019*	*0.016*	na	*0.023*	*0.041*	na	*0.022*	na	*0.025*	na	na	na
Th	*0.036*	*0.015*	*0.175*	*0.025*	na	*0.049*	*0.062*	na	*0.114*	na	*0.011*	na	na	na
U	*0.072*	*0.025*	*0.084*	*0.019*	na	*0.111*	*0.030*	na	*0.069*	na	*0.012*	na	na	na

Sample	TL-116	TL-117	TL-118	TL-119	TL-120	TL-121	TL-123	TL-124	TL-125	TL-126	TL-129	TL-130	TL-133	TL-134
Rock Type	1	1	1	1	1	3	2	1	2	2	2	2	3	3
Texture	M	PtM	M	PtM	PrtP	M	PtM	P	M	PrtP	PrtP	PrtP	PrtM	P
SiO_2 wt.%	45.00	44.60	45.30	44.4	44.90	41.30	45.90	45.30	45.90	45.20	45.10	44.50	41.10	41.30
TiO_2	0.06	0.06	0.05	0.086	0.10	0.05	0.05	0.06	0.09	0.05	0.05	0.08	0.04	0.04
Al_2O_3	1.71	1.65	1.21	2.13	2.84	0.38	2.10	2.43	1.26	1.02	1.25	1.37	0.30	0.32
$Fe_2O_3^a$	8.80	8.80	8.70	8.4	8.80	8.10	8.60	8.20	8.70	9.10	9.00	8.30	8.60	9.90
MnO	0.12	0.13	0.13	0.12	0.12	0.11	0.12	0.12	0.13	0.13	0.13	0.12	0.11	0.13
MgO	43.60	42.90	44.30	43.5	40.80	50.00	41.80	41.80	42.50	44.30	44.10	45.00	49.70	48.30
CaO	1.32	2.52	0.82	1.85	2.94	0.32	2.21	2.47	2.03	0.85	0.94	1.10	0.36	0.35
Na_2O	0.14	0.10	0.12	0.130	0.15	0.06	0.10	0.08	0.16	0.14	0.12	0.09	0.07	0.08
K_2O	0.02	0.01	0.01	0.002	0.002	0.01	<0.001	0.01	0.03	0.02	0.03	0.004	0.03	0.01
Total	100.69	100.70	100.63	100.56	100.58	100.23	100.83	100.40	100.70	100.76	100.70	100.56	100.23	100.39
mg#	90.8	90.7	91.1	91.2	90.3	92.5	90.7	91.1	90.8	90.6	90.7	91.5	92.1	90.7
Sc ppm	4.4	9.5	8.3	6.7	8	2.4	8	8.2	8.1	6.5	6.6	6.4	0.7	2.1
V	41	47	29	47	60	13	45	41	51	30	32	33	14	16
Cr	2395	2908	2819	2563	2498	2865	2586	3178	3051	2463	2613	2240	2738	2142
Co	106	102	106	103	99	118	101	103	97	108	109	106	121	126
Ni	2287	2283	2136	2322	2117	2825	2219	2184	2223	2253	2360	2397	2694	2733
Zn	46	49	45	46	45	43	44	45	46	46	45	43	44	45
Ga	2.3	2.3	2.3	3	3.6	1.8	0.5	2.1	2.9	1.7	1.7	2	0.8	0.8
Rb	0.2	0.3	0.7	0.1	0.4	0	0.1	0.3	0.6	0.6	0.4	0.4	0.2	0.6
Sr	4.1	5.5	4.2	4.3	4.4	4.4	1.1	3.8	5.6	3.5	5	3.3	5.2	7.8
Y	0.5	0.3	0.2	1.3	1.8	0.2	0.6	1.4	1.4	0.6	1.1	0.1	0.2	
Zr	3.6	0.7	3.1	3.9	2.8	1.8	1.9	1.2	7.3	0.6	4.0	3.3	6.0	1.2
La	*0.329*	na	*0.225*	*0.088*	*0.229*	*0.189*	*0.047*	*0.201*	*0.172*	*0.072*	*0.338*	*0.329*	*0.709*	*0.616*
Ce	*0.470*	na	*0.467*	*0.241*	*0.700*	*0.359*	*0.102*	*0.458*	*0.416*	*0.110*	*0.630*	*0.574*	*1.080*	*1.849*
Pr	*0.053*	na	*0.031*	*0.043*	*0.104*	*0.034*	*0.012*	*0.063*	*0.046*	*0.016*	*0.078*	*0.095*	*0.103*	*0.254*
Nd	*0.205*	na	*0.105*	*0.246*	*0.473*	*0.123*	*0.054*	*0.314*	*0.179*	*0.072*	*0.275*	*0.398*	*0.319*	*0.881*
Sm	*0.058*	na	*0.021*	*0.107*	*0.159*	*0.028*	*0.020*	*0.122*	*0.049*	*0.020*	*0.060*	*0.117*	*0.056*	*0.062*
Eu	*0.021*	na	*0.008*	*0.045*	*0.063*	*0.008*	*0.008*	*0.050*	*0.017*	*0.008*	*0.017*	*0.041*	*0.017*	*0.016*
Gd	*0.080*	na	*0.028*	*0.181*	*0.288*	*0.031*	*0.042*	*0.200*	*0.065*	*0.030*	*0.068*	*0.155*	*0.057*	*0.058*
Tb	*0.014*	na	*0.005*	*0.034*	*0.054*	*0.005*	*0.010*	*0.038*	*0.012*	*0.005*	*0.013*	*0.027*	*0.008*	*0.010*
Dy	*0.089*	na	*0.031*	*0.228*	*0.374*	*0.026*	*0.083*	*0.264*	*0.077*	*0.038*	*0.083*	*0.163*	*0.041*	*0.058*
Ho	*0.020*	na	*0.007*	*0.050*	*0.088*	*0.006*	*0.022*	*0.059*	*0.018*	*0.009*	*0.019*	*0.036*	*0.009*	*0.013*
Er	*0.064*	na	*0.025*	*0.152*	*0.258*	*0.017*	*0.072*	*0.178*	*0.056*	*0.030*	*0.063*	*0.103*	*0.026*	*0.042*
Tm	*0.011*	na	*0.005*	*0.023*	*0.039*	*0.003*	*0.012*	*0.027*	*0.009*	*0.005*	*0.010*	*0.016*	*0.005*	*0.007*
Yb	*0.072*	na	*0.032*	*0.147*	*0.250*	*0.021*	*0.083*	*0.170*	*0.059*	*0.035*	*0.067*	*0.100*	*0.032*	*0.048*
Lu	*0.012*	na	*0.006*	*0.024*	*0.038*	*0.004*	*0.014*	*0.026*	*0.010*	*0.006*	*0.011*	*0.016*	*0.006*	*0.009*
Th	*0.045*	na	*0.060*	*0.059*	*0.083*	*0.032*	*0.011*	*0.050*	*0.042*	*0.029*	*0.142*	*0.091*	*0.296*	*0.111*
U	*0.198*	na	*0.056*	*0.056*	*0.031*	*0.033*	*0.015*	*0.055*	*0.021*	*0.026*	*0.072*	*0.043*	*0.070*	*0.052*

Rock type and texture as in Table 1a.

[a] Fe total as Fe2O3; italic numbers ICP-MS, otherwise XRF analyses.

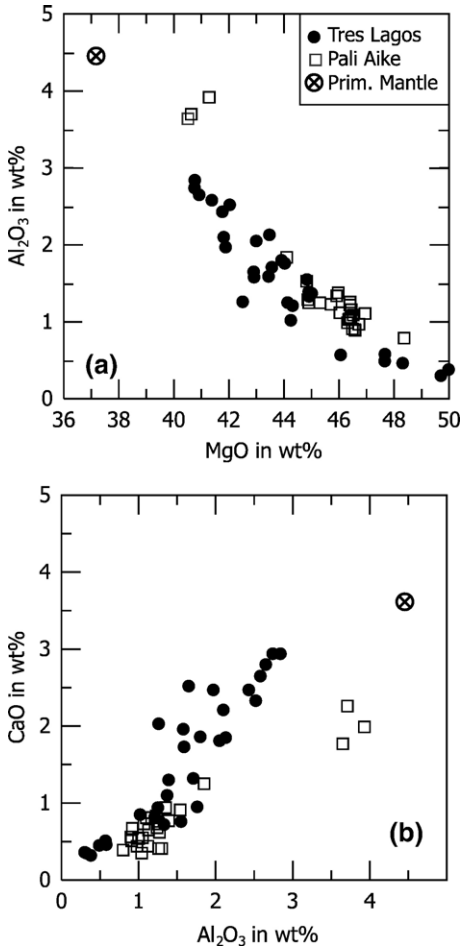

Fig. 7. Variation plots of bulk contents of Al_2O_3, MgO and CaO (wt.%) in Tres Lagos and Pali Aike xenoliths: a) contents of Al_2O_3 vs. MgO, b) contents of CaO vs. Al_2O_3. Pali Aike from Stern et al. (1999), PM of McDonough and Sun (1995).

4.5.2. Metasomatism beneath Tres Lagos

From the studied samples it is evident that the mantle lithosphere below Tres Lagos represents residual depleted mantle and that metasomatism was not a significant process. The absence of hydrous phases like amphibole and/or phlogopite precludes to a certain degree modal metasomatism although in the most depleted rocks, as is the case of the dunites (sample TL-133), LREE-enriched clinopyroxenes are the result of modal metasomatism (Fig. 5a, b).

As cpx is the major repository for REE, the whole rock REE patterns should resemble those of cpx. This is the case only for non-metasomatized peridotites. The whole rock metasomatized peridotites show patterns with elevated LREE abundances, whereas their clinopyroxenes have patterns that are depleted in LREE. These contrasting LREE patterns appear to be the result of host basalt infiltration during and/or maybe after the xenoliths were entrained by the basalts on the way to the surface. If the whole rock LREE enrichment took place before the uplift of the xenoliths by the host lavas, one would expect that clinopyroxenes would show typical "spongy" rims as response to the introduction of fluids/melts and subsequent decompression during their transport to the surface. The fact that "spongy" clinopyroxenes are scarce strongly supports that melts/fluids were introduced "en-route" to the surface and therefore without enough time for their reaction with clinopyroxenes. Host basalt infiltration is described by Schilling et al. (2005) for similar anhydrous xenoliths from Cerro Redondo, a locality approximately 110 km ENE of Tres Lagos (Fig. 1). However, Cerro Redondo xenoliths have been strongly modified by host basalt infiltration (Schilling et al., 2005), whereas Tres Lagos xenoliths do not show evidence for considerable modifications due to host basalt infiltration (glass veinlets and spongy cpx are only present occasionally).

Simple mass balance calculations between whole rock and cpx have been performed for Sr and Nd on samples with available whole rock Sr and Nd isotopic data (Table 3). The results show that the Sr excess is merely located in the grain boundaries. While an excess of Nd in the metasomatized samples is located in the grain boundaries, the calculations on the non-metasomatized samples TL-104 and TL-111 are very similar to the corresponding whole rock analyses (Table 3). The radiogenic Sr and Nd isotopes are consistent with the above observations. For the non-metasomatized samples TL-104 and TL-111 a decoupling of Sr from Nd is evident. In these samples the unusually high Sr isotopes are not accompanied by low Nd isotopes. The high Sr isotopic ratios could be either the result of host basalt infiltration or mixing with Sr-rich material. Host basalt infiltration can be excluded since $^{86}Sr/^{87}Sr$ ratio of basalts from Meseta Central (Gorring and Kay, 2001) and Tres Lagos (Stern et al., 1990) is lower than those of the TL-104 and TL-111 xenolith samples (Fig. 9). Since there are no other phases present, it is most likely that the high Sr-isotopes could be derived after contamination with ground-water or/and surface Ca-rich solutions. Similar observations are reported by Xu et al. (2003) for the Southeastern China xenoliths. The metasomatized samples that plot close to the MCB isotopic field (Fig. 9) reflect first host basalt infiltration and subsequent contamination by ground water or/and Ca-rich surface solutions.

4.5.3. Tectonic implications

Tres Lagos belongs to the Meseta Central which is situated inboard of the active continental margin (Ramos, 1999; Gorring and Kay, 2001) between the SVZ and the

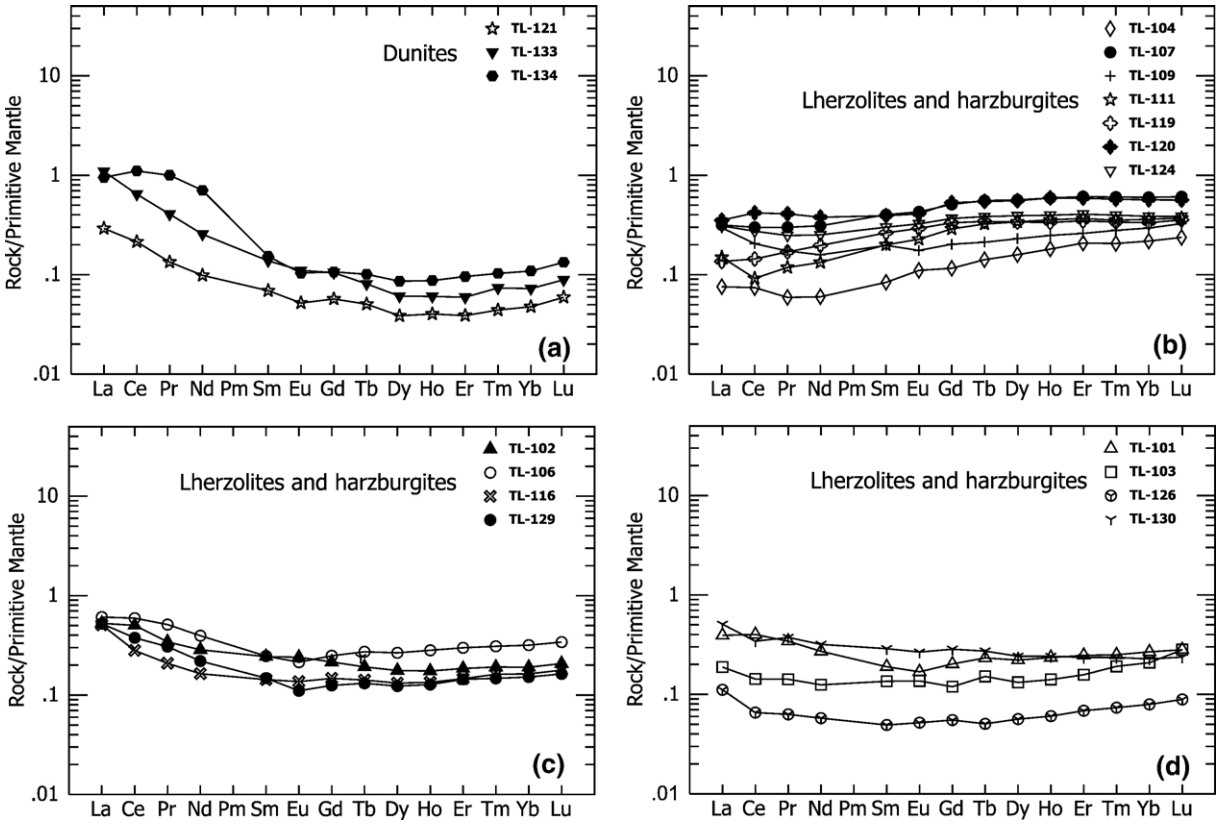

Fig. 8. Primitive mantle normalized bulk REE concentration patterns of Tres Lagos xenoliths. a) LREE enriched dunites, b) LREE depleted lherzolites and harzburgites c) LREE enriched lherzolites and harzburgites, d) lherzolites and harzburgites with U-shaped patterns. PM-normalizing values from McDonough and Sun (1995).

AVZ, which is characterized by the absence of modern active arc volcanism (Fig. 1) This volcanic gap has been interpreted as the result of the collision of a Chile Ridge segment with the Chile Trench, with subsequent formation of a 'slab-window' which in turn influenced the back-arc magmatic activity (Gorring and Kay, 2001 and references therein). Slab-window basaltic magmas are the product of decompression melting as asthenospheric mantle upwells through the gap that opens between the subducting oceanic plates as a ridge system is subducted or overridden by the hanging-wall plate (Thorkelson and Taylor, 1989). According to this model, it is expected that the mantle lithospheric wedge will be affected by fluids/melts released from the subducted slab during its passage below the mantle lithosphere from which the studied xenoliths originate. However, the Tres Lagos xenoliths,

Table 3
Bulk rock Sr and Nd isotopic ratios

Sample	Rock type	Texture	Rb	Sr	$^{87}Rb/^{86}Sr$	$^{87}Sr/^{86}Sr$	±2 σ	Sm	Nd	$^{147}Sm/^{144}Nd$	$^{143}Nd/^{144}Nd$	±2 σ	Sr*	Sm*	Nd*
TL-101	1	PtM	0.7	3.8	0.5328	0.704767	0.000028	0.077	0.339	0.1373	0.512888	0.000024	2.0	0.042	0.084
TL-103	2	PtM	0.7	3.1	0.6531	0.704403	0.000023	0.055	0.156	0.2132	0.512904	0.000024	2.2	0.031	0.065
TL-104	2	PtM	0.5	2.4	0.6026	0.705506	0.000014	0.034	0.075	0.2741	0.513043	0.000020	0.8	0.036	0.058
TL-106	1	PtM	0.6	2.7	0.6428	0.705994	0.000016	0.100	0.494	0.1224	0.512877	0.000022	1.1	0.049	0.086
TL-109	1	PtM	0.5	3.5	0.4132	0.704549	0.000014	0.080	0.198	0.2440	0.512883	0.000020	2.0	0.072	0.096
TL-111	1	PtM	0.7	3.4	0.5955	0.705090	0.000008	0.091	0.166	0.3315	0.513118	0.000010	1.0	0.108	0.137
TL-116	1	M	0.2	4.1	0.1411	0.704508	0.000004	0.058	0.205	0.1711	0.512814	0.000044	2.9	0.047	0.098
TL-133	3	PrtM	0.2	5.2	0.1113	0.705817	0.000010	0.056	0.319	0.1061	0.512733	0.000008	3.5	0.017	0.066

Sr*, Sm* and Nd* contents from mass balance calculations.
Rb has not been calculated due to inaccurate LA-ICP-MS analyses. Rock type and texture as in Table 1a.

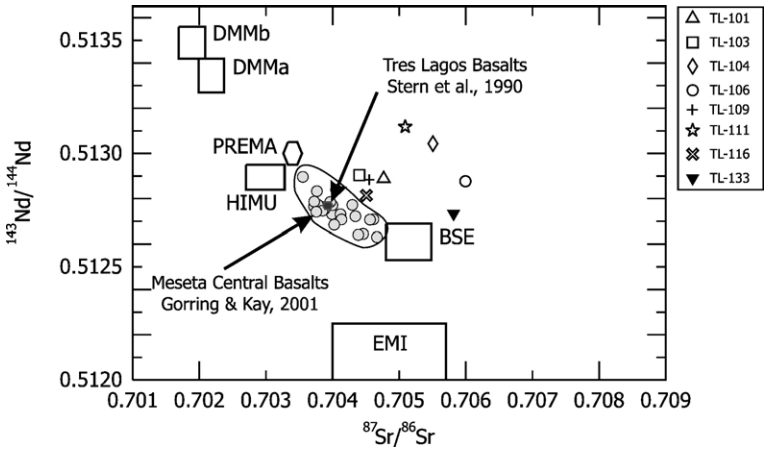

Fig. 9. Bulk rock Sr–Nd isotopes from selected Tres Lagos xenoliths. Isotopic ratios from Meseta Central basalts (Gorring and Kay, 2001) and Tres Lagos basalts (Stern et al., 1990) are also plotted. Mantle reservoirs after Zindler and Hart (1986).

like those from Cerro Redondo (Schilling et al., 2000), Lote 17 (Gorring and Kay, 2000) and Pali Aike (Stern et al., 1999), show that subduction-related fluids/melts did not affect the mantle wedge. In contrast, xenoliths from Lote 17, which is located 72 km north of Cerro Redondo and 150 km NE of Tres Lagos, show that the lithosphere has been heavily affected by modal and cryptic carbonatitic metasomatism that is not attributed to subduction slab-related fluids/melts (Gorring and Kay, 2000). Two possibilities could account for the absence of metasomatism: a) the 'slab-window' model does not apply and b) Tres Lagos xenoliths represent a fragment of isolated old lithosphere. It is likely that the 'slab-window' model does not apply because, as mentioned above, the mantle lithosphere beneath Tres Lagos, Lote 17 and Cerro Redondo, which are all at the latitude of the VAG, have not been affected by subduction slab-related fluids/melts. Gorring et al. (1997) estimated a melt generation depth between ~60 to 80 km for Patagonian 'slab-window' lavas. Most of these lavas show evidence for components from the subducted slab and/or from the continental lithosphere and crust (Gorring and Kay, 2001). However the depth of ~60 km, corresponding a lithospheric pressure of ~17 Kb, is consistent with the equilibration depths estimated also for Tres Lagos xenoliths. Similar depths have been estimated for Lote 17 and Cerro Redondo xenoliths. It is therefore difficult to explain why the supra-slab mantle beneath these localities remained immune, i.e. was not affected by melt/fluids circulation during the evolution of a 'slab-window'. The only known mantle xenoliths modified by metasomatic fluids/melts derived from subducted slab are those from Cerro del Fraile, an outcrop located less than 25 km from the Andean SVZ and not in the VAG (Fig. 1 and Kilian and Stern, 2002). Therefore, if the 'slab-window' model does not apply, then other mechanisms need to be invoked in order to explain the volcanic gap. But even if the 'slab-window' model applies, the second possibility is strongly supported by the fact that the Tres Lagos xenoliths in the Fo versus modal olivine abundance (Fig. 13) plot within the Proterozoic field (Griffin et al., 2003). Their depletion in basaltic components and the low P-T conditions that correspond to a relative cold environment at shallow depths support the possibility that xenoliths from Tres Lagos were sampled from an old isolated lithospheric mantle. An argument against the isolated old lithospheric mantle might be the fact that Proterozoic crust is, up to now, not known in the area of Tres Lagos. However, the basement in the central and NE sector of the VAG, consists of old metamorphic rocks of latest Proterozoic (540±60 Ma; Pezzuchi, 1978)

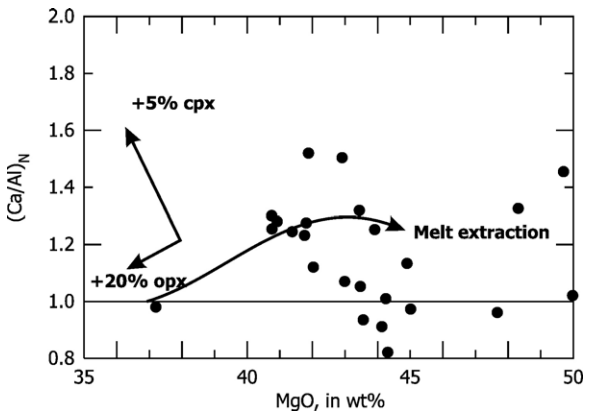

Fig. 10. The effect of melt extraction in combination with modal composition heterogeneity on the Ca/Al ratio of the Tres Lagos xenoliths (adapted from O'Neill and Palme, 1998).

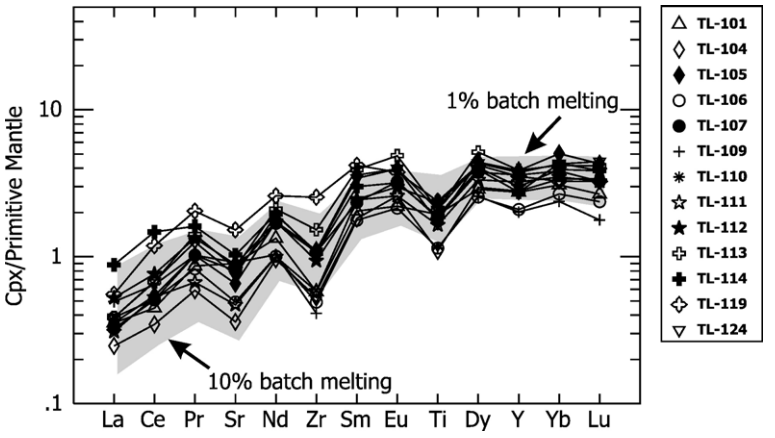

Fig. 11. Model calculations (shadow area) show that residual clinopyroxene incompatible trace element abundances are the result of two stage batch melting process. A 2% of batch melting of a PM in the garnet peridotite field is the source for subsequent 2–8% batch melting in the spinel peridotite field. PM values from McDonough and Sun (1995).

to Grenville age (1100 Ma; Pankhurst et al., 1994), both units belonging to the Macizo del Deseado (Fig. 1).

5. Conclusions

The Tres Lagos xenoliths are mainly spinel lherzolites and harzburgites depleted in basaltic components. Among them there is a group of only a few samples that have experienced modal and cryptic metasomatism. The non-metasomatized depleted samples represent the residues of peridotites that have experienced about 2% of batch melting in the garnet peridotite field and subsequently 2–8% batch melting in the spinel peridotite field. This group has concave downwards clinopyroxene REE abundance patterns, whereas their corresponding whole rock patterns generally show LREE enrichments, indicating host basalt infiltration. Radiogenic whole rock Sr and Rb isotopic ratios reflect a more complex mixing history. A number of samples show that host basalt infiltration affected the whole rock Sr and Nd isotopic ratios. Subsequently ground water and/or circulation of surface carbonatic solutions caused an unusual increase of the $^{86}Sr/^{87}Sr$ in all samples. The Tres Lagos xenoliths probably represent an old isolated piece of depleted lithosphere, in which metasomatism was not a significant process.

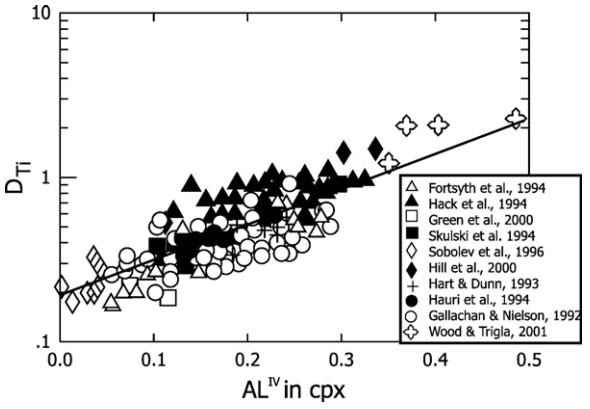

Fig. 12. Partition coefficients for selected trace elements plotted against the number of tetrahedral aluminum atoms (Al^{IV}) in clinopyroxene per formula unit. Data are taken from experiments performed on (ultra)basic liquids compositions at a broad range of temperature (1050–1430 °C) and pressure (0.001–40 kb). Data from Forsythe et al. (1994), Gallahan and Nielsen (1992), Hack et al. (1994), Hart and Dunn (1993), Hauri et al. (1994), Hill et al. (2000), Skulski et al. (1994), Sobolev et al. (1996), Wood and Trigila (2001).

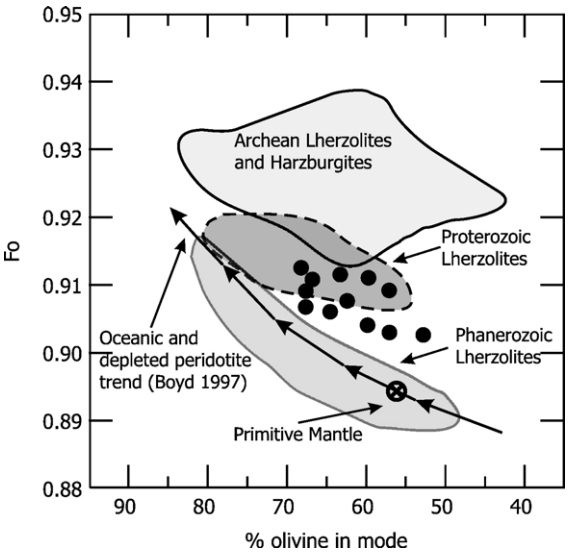

Fig. 13. Modal olivine content versus Fo content in Tres Lagos xenoliths. Primitive mantle after McDonough and Sun (1995), fields after Griffin et al. (2003), oceanic and depleted peridotite trend after Boyd (1997).

Acknowledgements

This work was supported by ANPCYT (Argentina) Grant BID 1201/OC-AR — PICT N° 07-11791 to E.A. B. Th. N acknowledges the support of the European Community Access to Research Infrastructure action of the Improving Human Potential Programme, contract HPRI-CT-1999-00008 awarded to B. J. Wood (EU Geochemical Facility, University of Bristol). Martin Thöni for the Sr and Nd isotope analyses and Peter Nagl for XRF analyses, both from the University of Vienna, are gratefully acknowledged. We thank Michel Gregoire and Charles Stern for their constructive comments and suggestions on the manuscript and Hilary Downes for improving the English.

References

Bjerg, E.A., Ntaflos, Th., Kurat, G., Dobosi, G., Labudia, C.H., 2005. The upper mantle beneath Patagonia, Argentina, documented by xenoliths from alkali basalts. J. South Am. Earth Sci. 18 (2), 125–142.

Boyd, F.R., 1997. Origin of peridotite xenoliths: major element considerations. In: Ranalli, G., Lucchi, F.R., Ricci, CA., Trommsdorff, T. (Eds.), High Pressure and High Temperature Research on Lithosphere and Mantle Materials. University of Siena, Siena.

Brey, G.P., Köhler, T., 1990. Geothermobarometry in four phase lherzolite II. New thermobarometers, and practical assessment of existing thermobarometers. J. Petrol. 31, 1353–1378.

Forsythe, L.M., Nielson, R.L., Fisk, M.R., 1994. High-field-strength element partitioning between pyroxene and basaltic to dacitic magmas. Chem. Geol. 117, 107–125.

Frey, F.A., Suen, C.J., Stockman, H.W., 1985. The Ronda high temperature peridotite: geochemistry and petrogenesis. Geochim. Cosmochim. Acta 49, 2469–2491.

Gallahan, W.E., Nielsen, R.L., 1992. The partitioning of Sc, Y, and rare earth elements between high-Ca pyroxene and natural mafic to intermediate lavas at 1 atmosphere. Geochim. Cosmochim. Acta 56, 2387–2404.

Gorring, M.L., Kay, S.M., 2000. Carbonatite metasomatized peridotite xenoliths from southern Patagonia: implications for lithospheric processes and Neogene plateau magmatism. Contrib. Mineral. Petrol. 140, 55–72.

Gorring, M.L., Kay, S.M., 2001. Mantle processes and source of neogene slab window magmas from southern Patagonia, Argentina. J. Petrol. 42, 1067–1094.

Gorring, M.L., Kay, S.M., Zeitler, P.K., Ramos, V.A., Rubiolo, D., Fernandez, M.I., Panza, J.L., 1997. Neogene Patagonian plateau lavas: continental magmas associated with ridge collision at the Chile triple junction. Tectonics 16, 1–17.

Green, T.H., Blundy, J.D., Adam, J., Yaxley, G.M., 2000. SIMS determination of trace element partition coefficients between garnet, clinopyroxene and hydrous basaltic liquids at 2–75 GPa and 1080–1200 C. Lithos 53, 165–187.

Griffin, W.L., Reilly, S.Y., Abe, N., Aulbach, S., Davies, R.M., Pearson, N.J., Doyle, B.J., Kivi, K., 2003. The origin and evolution of Archean lithospheric mantle. Precambrian Res. 127, 19–41.

Hack, P.J., Nielsen, R.L., Johnston, A.D., 1994. Experimentally determined rare-earth element and Y partitioning behavior between clinopyroxene and basaltic liquids at pressures up to 20 Kbar. Chem. Geol. 117, 89–105.

Hart, S.R., Dunn, T., 1993. Experimental cpx/melt partitioning of 24 trace elements. Contrib. Mineral. Petrol. 113, 1–8.

Hauri, E.H., Wagner, T.P., Grove, T.L., 1994. Experimental and natural partitioning of Th, U, Pb and other trace elements between garnet, clinopyroxene and basaltic melts. Chem. Geol. 117, 149–166.

Hill, E., Wood, B.J., Blundy, J.D., 2000. The effect of Ca–Tschermaks component on trace element partitioning between clinopyroxene and silicate melt. Lithos 53, 203–215.

Johnson, K.T.M., Dick, H.J.B., Shimizu, N., 1990. Melting in the oceanic upper mantle: an ion microprobe study of diopside in abyssal peridotites. J. Geophys. Res. 95, 2661–2678.

Kilian, R., Stern, C.R., 2002. Constraints on the interaction between slab melts and the mantle wedge from adakitic glass in peridotite xenoliths. Eur. J. Mineral 14, 25–36.

Kilian, R., Franzen, Ch., Koch, M., 1998. The metasomatism of the mantle wedge below the southern Andes: constraints from laser ablation microprobe ICP-MS trace element analysis of clinopyroxenes, orthopyroxenes and fluid inclusions of mantle xenoliths. Terra Nostra 98 (5), 81.

Köhler, T., Brey, G.P., 1990. Ca-exchange between olivine and clinopyroxene as a geothermobarometer calibrated from 2 to 60 Kbar in primitive natural lherzolites. Geochim. Cosmochim. Acta 54, 2375–2388.

McDonough, W.F., Sun, S., 1995. The composition of the Earth. Chem. Geol. 120, 223–253.

Mercier, J.C.C., Benoit, V., Girardeau, J., 1984. Equilibrium state of diopside-bearing harzburgites from ophiolites: geobarometric and geodynamic implications. Contrib. Mineral. Petrol. 85, 391–403.

Mercier, J.C.C., Nicolas, A., 1975. Textures and fabrics of upper-mantle peridotites as illustrated by xenoliths from basalts. J. Petrol. 16 (2), 454–487.

Niu, Y., Batiza, R., 1991. An empirical method for calculating melt compositions produced beneath mid-ocean ridges: application for axis and off-axis (seamounts) melting. J. Geophys. Res. 96, 21753–21777.

Norman, M.D., 1998. Melting and metasomatism in the continental lithosphere: laser ablation ICPMS analysis of minerals in spinel lherzolites from eastern Australia. Contrib. Mineral. Petrol. 130, 240–255.

Ntaflos, Th., Bjerg, E.A., Labudía, 2002. High temperature, low pressure garnet-peridotites from Praguaniyen: evidence for plume activity in northern Patagonia. Actas XV congresso Geologico Argentina, vol. 3, pp. 53–55.

O'Neill, H., Palme, H., 1998. Composition of the silicate Earth: implications for accretion and core formation. In: Jackson, I. (Ed.), The Earth's Mantle: Composition, Structure and Evolution. Cambridge University Press, pp. 3–126.

Pankhurst, R.J., Hervé, F., Rapela, C.W., 1994. Sm–Nd evidence for the Grenvillian provenance of the metasedimentary basement of southern Chile and west Antarctica. Actas VII Congreso Geológico Chileno, vol. 2, pp. 1414–1418.

Pezzuchi, H., 1978. Estudio geológico de la zona de Estancia Dos Hermanas — Estancia 25 de Mayo y adyacencias, Departamento Deseado, provincia de Santa Cruz. Ph.D. dissertation, Universidad Nacional de La Plata, La Plata, Argentina. Unpublished.

Ramos, V.A., 1999. Plate tectonic setting of the Andean Cordillera. Episodes 22 (3), 183–190.

Rivalenti, G., Mazzucchelli, M., Laurora, A., Ciuffi, S., Zanetti, A., Vannucci, R., Cingolani, C.A., 2004. The backarc mantle lithosphere in Patagoia, South America. J. South Am. Earth Sci. 17, 121–152.

Schilling, M., Conceicao, R.V., Mallmann, G., Koester, E., Kawashita, K., Herve, F., Morata, D., Motoki, A., 2005. Spinel-facies mantle xenoliths from Cerro Redondo, Argentine Patagonia: petrographic, geochemical, and isotopic evidence of interaction between xenoliths and host basalt. Lithos 82, 485–502.

Skulski, T., Minarik, W., Watson, E.B., 1994. High-pressure experimental trace-element partitioning between clinopyroxene and basaltic melts. Chem. Geol. 117, 127–147.

Sobolev, A.V., Migdisov, A.A., Portnyagin, M.V., 1996. Incompatible elements partitioning between clinopyroxene and basaltic melt based on the study of melt inclusions in minerals from Troodos, Cyprus. Petrology 4, 307–317.

Stern, C.R., 2004. Active Andean volcanism: its geologic and tectonic setting. Rev. Geol. Chile 31 (2), 161–206.

Stern, C.R., Kilian, R., 1996. Role of the subducted slab, mantle wedge and continental crust in the generation of adakites from the Andean Austral Volcanic Zone. Contrib. Mineral. Petrol. 123, 263–281.

Stern, C.R., Frey, F.A., Futa, K., Zartman, R.E., Peng, Z., Kyser, T.K., 1990. Trace-element and Sr, Nd, Pb, and O isotopic composition of Pliocene and Quaternary alkali basalts of the Patagonian Plateau lavas of southernmost South America. Contrib. Mineral. Petrol. 104, 294–308.

Stern, C.R., Kilian, R., Olker, B., Hauri, E.H., Kyser, T.K., 1999. Evidence from mantle xenoliths for relatively thin (<100 km) continental lithosphere below the Phanerozoic crust of southernmost South America. Lithos 48, 217–235.

Thöni, M., Miller, Ch., 2004. Ordovician meta-pegmatite garnet (N-W Ötztal basement, Tyrol, Eastern Alps): preservation of magmatic garnet chemistry and Sm–Nd age during mylonitization. Chem. Geol. 209, 1–26.

Thorkelson, D.J., Taylor, R.P., 1989. Cordilleran slab windows. Geology 17, 833–836.

Wood, B.J., Trigila, R., 2001. Experimental determination of aluminous clinopyroxene-melt partition coefficients for potassic liquids, with application to the evolution of the Roman province potassic magmas. Chem. Geol. 172, 213–223.

Xu, X., O'Reilly, S.Y., Griffin, W.L., Zhou, X., 2003. Enrichment of upper mantle peridotite: petrological, trace element and isotopic evidence in xenoliths from SE China. Chem. Geol. 198 (3–4), 163–188.

Xu, X., O'Reilly, S.Y., Griffin, W.L., Zhou, X., 2000. Genesis of young lithospheric mantle in southeastern China: a LAM-ICPMS trace element study. J. Petrol. 41, 111–148.

Zindler, A., Hart, S.R., 1986. Chemical geodynamics. Annu. Rev. Earth Planet. Sci. 14, 493–571.